Transparent Near-IR Dye-Sensitized Solar Cells: Ultrafast Spectroscopy Reveals the Effects of Driving Force and Dye Aggregation

Mate Kurucz, Ilias Nikolinakos, Jimmy Soueiti, Thibaut Baron, Fionnuala Grifoni, Waad Naim, Yann Pellegrin, Frederic Sauvage, Fabrice Odobel, Stefan Haacke

RESEARCH ARTICLE

Transparent Near-IR Dye-Sensitized Solar Cells: Ultrafast Spectroscopy Reveals the Effects of Driving Force and Dye Aggregation

Mate Kurucz,[a]$ Ilias Nikolinakos,[a]$ Jimmy Soueiti,[a] Thibaut Baron, [b] Fionnuala Grifoni, [c] Waad Naim, [c]£ Yann Pellegrin, [b], Frédéric Sauvage, *[c] Fabrice Odobel, *[b] and Stefan Haacke*[a]

[a] Dr. I. Nikolinakos, Dr. M. Kurucz, J. Soueiti, Pr. S. Haacke
Inst. de Physique et Chimie des Matériaux (IPCMS)
University of Strasbourg - CNRS
23, Rue du Loess; 67034 Strasbourg, France
E-mail: stefan.haacke@ipcms.unistra.fr

[b] Dr. T. Baron, Dr. Y. Pellegrin, Dr. F. Odobel
Nantes Université, CNRS, CEISAM, UMR 6230
F-44000 Nantes, France
E-mail: Fabrice.Odobel@univ-nantes.fr

[c] Dr. F. Grifoni, Dr. W. Naim, Dr. F. Sauvage
Laboratoire de Réactivité et Chimie des Solides
Université de Picardie Jules Verne . CNRS
Hub de l'énergie, 15 Rue Baudelocque, 80000 Amiens, France
E-mail: frederic.sauvage@u-picardie.fr

$ These authors contributed equally

£ Present affiliation: Dept. Chem. Eng.& Mat. Sc., Michigan State University, East Lansing, USA

Supporting information for this article is given via a link at the end of the document.

Abstract: In the context of developing transparent near-IR absorbing dye-sensitized solar cells, diketopyrrolopyrrole (DPP) cyanine dyes have recently emerged as an alternative to strongly aggregating linear cyanines. In our efforts to increase both the power conversion efficiency (PCE) and the average visible transmittance (AVT), a thienylated version, called **TB202**, that shows a red-shifted absorption with respect to our champion dye **TB207** was designed. However, the lower energy LUMO level of **TB202** brings along a lower driving force (-ΔG) for carrier injection, which we recently identified as the main parameter limiting the PCE to 1.5% in the best device conditions. In the present paper, we publish a detailed account of the effect of the de-aggregating cheno-deoxycholic acid (CDCA) for both **TB207** and **TB202**. Both transient absorption (TAS) and fluorescence up-conversion (FLUPS) data are presented, which allow to quantitively compare the effect of -ΔG and the CDCA concentration, in terms of the kinetic competition of ensemble averaged carrier injection and monomer-to-aggregate energy transfer (ET) rates. A comprehensive picture emerges on how ET is reduced by higher CDCA concentrations, leading in the best device conditions to injection efficiencies in the range of 65% for **TB207** and only 35% for **TB202**.

Introduction

It goes without saying that photo-voltaics is a key technology for renewable and sustainable production of electricity and solar fuels. R&D in this area is extremely active with the aim of combining highest power conversion efficiencies (PCE), with low production costs and long-term durability of the solar cells (SC). Third generation solar cells, based on perovskites, organic molecular systems or hybrid solutions, such as dye-sensitized solar cells (DSSCs) need to mature more in terms of long-term stability, but they are already explored for alternative modes of usage (e.g. integration in tissue) or large scale deployment approaches, like "building-integrated PV"[1,2]. For the latter in particular, a very appealing prospect is the development of transparent and colorless solar cells, the active materials of which absorb only the invisible near-UV[3] and near-IR parts of the sun's spectrum. Since 45% of sunlight radiation received on Earth lies in the near-IR (λ≤1700nm), this part of the spectrum is presently targeted by the development of selectively near-IR absorbing solar cells (SCs), based either on organic photovoltaics (OPV)[1,4] or on DSSCs [5–7]. The transparency of the SCs is evaluated by the "average visible transmission" (AVT). For aesthetic reasons, the transparent see-through SCs should not alter the colors of transmitted images, which is quantitatively evaluated by the "color rendering index" (CRI). The most successful devices combine all three metrics, or maximizes at least the product AVT X PCE = LUE, the "Light Utilization Efficiency"[8]. The state-of-the-art in the development of materials (dyes, electrolytes, anodes, etc.) for transparent DSSCs was recently and comprehensively reviewed[9].

Increasing AVT goes at the expense of PCE, in particular for non-wavelength selective absorbers: The theoretical PCE limit of a 100% AVT single junction cell using wavelength-selective transparent photovoltaics (TPV) technology, i.e. combining UV-

selective and NIR-selective absorption, is 20.5%[8], lower than the Schottky-Queisser limit for UV/VIS/near-IR absorbing semi-conductors. In practice, a lower 10.8% can only be expected after considering all optical losses from the selective conversion of the UV region and a reasonable long-wavelength limit of 950-1000nm for NIR dyes [8].

Among the wavelength-selective technologies, organic solar cells afford the highest LUE values of 2.2–3.7%, with PCEs ranging between 4 % and 10 %, and AVTs between 40 and 60 %[1,4]. Similar figures were achieved with DSSCs based on a squaraine dye (coded HSQ5) [10] with a 3.66 % PCE and a max. transmittance of 60 % at 560 nm. When the absorbance is further shifted into the near-IR part with cyanine dyes, we recently demonstrated a combination of PCE 3.1% and AVT 76% without any visible coloration[5] and AVT reaching above 80 % using thioate-based electrolyte[11]. Since, these cyanines have a strong tendency to form excited state quenching aggregates [12–16], our most recent development explored more bulky diketo pyrrolopyrrole (DPP) cyanines, such as **TB207**, the chemical structure of which is displayed in scheme 1. Here the best figures of merit were PCE= 3.9% and AVT= 76% [6]. With the aim of red-shifting the absorption spectrum further, and possibly increasing the electron injection driving force -ΔG [17,18], **TB202** was synthesized with thienyl groups at the place of phenyls at the bipyrrole unit (scheme 1). **TB202** displays indeed a 30nm-red shift of the absorption spectrum, and an improved AVT, but **TB202**'s LUMO level is only slightly above the TiO_2 conduction band edge, resulting in a small driving force of $-\Delta G$= 0.02 eV for electron injection[7], as compared to 0.10 eV for **TB207**[6]. These values determined by electrochemistry (cyclic voltammetry) for the dyes in solution do not represent the real values in the TiO_2 devices[19]. Indeed, the electronic energy levels of the TiO_2 conduction band down-shift due to the presence of 1M Li+ in the electrolyte by more than 100 meV [20–22], so that the nominal ΔG's become more negative for both dyes. But, since this down-shift does not depend on the nature of the dye adsorbed on the TiO_2, we assume that it is the same for both **TB207** and **TB202**.

In addition, and as it is well documented in the literature, dyes with a strong dipole moment have an additional effect on the energy of the conduction band that depends on the dipole direction[23,24]. The energy is decreased when the dipole moment is pointing away from the TiO_2 surface (positive dipole) and conversely when it is directed in the opposite direction. However, since **TB202** and **TB207** have a symmetric core structure their dipole moment is negligible both in the ground and excited state. A remaining but negligible small dipole remains due to the acid group grafting the dyes on TiO_2. In conclusion, it is reasonable to assume that the difference of the ΔG values determined by electrochemistry (80 meV larger for **TB207**) is valid for device conditions as well.

This is reflected by the fact that the short-circuit current J_{sc} and the PCE are 2.5-times lower for **TB202** than for **TB207**, in the best device conditions[7]. Femtosecond transient absorption and spectroscopy showed that the carrier injection rate (monomer-to-TiO_2, CT) in **TB202** is indeed significantly smaller than in **TB207**, and that the competition with monomer-to-aggregate energy transfer (ET) limits the injection efficiency to ≤ 40% on the sub-ns time scale [7].

Ultrafast UV/VIS/near-IR spectroscopy is the method of choice for the study of the photo-induced processes in DSSCs as it provides a direct insight into electron injection rates and efficiencies, as well as possible geminate recombination processes[25]. The reader is referred to sound review articles[15,25–27] as well as to the early papers reporting on ultrafast spectroscopy in spectral domains ranging from UV/VIS to THz, and on a variety of organic and organometallic dyes[28–34]. Of particular interest is the detrimental effect of dye aggregates on the injection rates and yields, which was already reported for red- or near-IR absorbing dyes[12–14,35–38].

In the present paper, we present a detailed comparison of the ultrafast spectroscopy[15] of both dyes isolated as monomers in solution, or as a heterogeneous monomer-aggregate mixture in full devices grafted on the TiO_2 and Al_2O_3 photo-electrodes. For the latter the spectroscopic and kinetic properties of the aggregates are of particular interest, but they were less scrutinized before. Hence, we present a detailed comparison of monomer-to-aggregate energy transfer kinetics and its competition with electron injection by monomers as a function of the concentration of the de-aggregating cheno-deoxycholic acid (CDCA). Femtosecond transient absorption (TAS) demonstrates indeed a crossover from ET to CT-dominated photo-physics as the CDCA concentration is increased. A particular point of interest is to understand how excited aggregates decay. Their spectral properties revealed by transient absorption suggest an inter-dimer charge transfer state to exist, as observed for other pyrrolopyrrole systems[38]. Finally, we discuss the possibility of electron injection, i.e. photo-current production by excited aggregates/dimers.

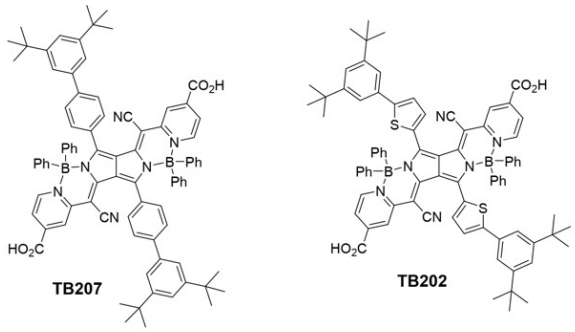

Scheme 1. Chemical structures of the DPP cyanine dyes **TB207** (left) and **TB202** (right).

Results and Discussion

Photo-physical properties of dye solutions

Figure 1 shows the steady-state absorption and fluorescence spectra of **TB202** and **TB207** in EtOH. As anticipated in the introduction, the thienyl units shift the absorption maximum by 30 nm into the red. The molar extinction coefficient is high (> $1.3x10^5$ M^{-1} cm^{-1}), due to $\pi-\pi^*$ transitions [6], and almost the same for both dyes. The fluorescence spectra are Stokes-shifted by 45 nm for **TB202** and 28 nm for **TB207**. **TB207** displays a good mirror-image symmetry with respect to the absorption spectra, as

expected for the rigid cyanide pyrrolopyrrole core of these dyes, on which HOMO and LUMO levels are localized [6,7]. The deviation in the vibrational progressions of absorption and emission is larger for **TB202**, indicating a more flexible conjugated structure.

The fluorescence decay times were measured with a time-gated streak camera (Hamamatsu C10627), as displayed in figure 2 A and B, for T**B207** and **TB202**, respectively.

We obtain the excited state lifetimes (ESL) by fitting a multi-exponential decay function convolved by the impulse response function of the system:

$$I(t) = \left[\sum_{k=0}^{n} \mathrm{A}_k \exp\left(-\frac{t}{\tau_k}\right)\right] * IRF(t) \qquad (1)$$

The IRF is the impulse response function of the setup, approximated by a Gaussian function.

The decay kinetics are wavelength-independent and are best fitted with a single time component. Based on this fitting the fluorescence lifetime is 3.1 ± 0.015 ns for **TB207** dye solution and 0.82 ± 0.01 ns for **TB202**. In contrast to **TB207, TB202**'s excited state lifetime is sub-ns, which is most likely due to internal conversion, in line with a more flexible structure. Indeed, as transient absorption data show (see below), no photo-product such as a triplet state is observed for ns delays.

Additional experiments were performed for both dyes in EtOH solution with broadband fluorescence up-conversion (150 fs time resolution), which highlight a progressive red-shift of the fluorescence spectrum due to excited state relaxation on a ≈ 30 ps time scale (see Figure S1 and S10). As an example, for **TB202** (fig. S10), a two-component exponential fitting was performed, which yielded lifetimes of 37 ps and 570 ps. The long lived component is similar to the value obtained by Streak camera (table 1).

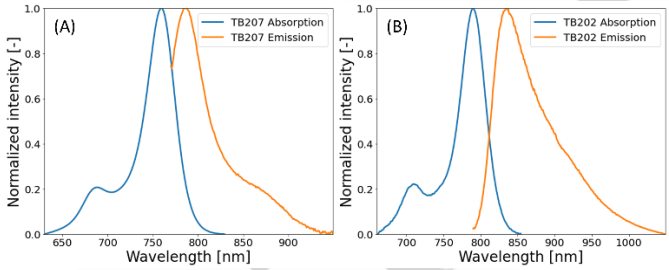

Figure 1. Normalized absorption and emission spectra of **TB207** (A) and **TB202** (B) in EtOH. The wavelength of maximum absorption is 30 nm red-shifted for **TB202**.

Most importantly, these experiments show that the intrinsic exc. state lifetimes (ESL) of these new dyes are much longer than usual lifetimes for charge injection (≤ 50 ps) [6], so that the spontaneous radiative or non-radiative S_1-S_0 relaxation is not in competition with the latter process central for the DSSC operation.

In addition to fluorescence decay times, it is important to record reference ΔA spectra for the isolated dyes in order to identify the characteristic bands and transition energies pertaining to S_1-S_n excited state absorption. Figure 3 presents the time-resolved TAS spectra at selected delay times for **TB207** (a) and **TB202** (b), obtained for excitation with 50 fs pulses at 750 and 770 nm, respectively. A wavelength interval of +/- 5 nm around the pump peak wavelength is not represented for TB207 due to residual pump light scattering. The shape of the ΔA spectra does not depend on the delay time, only their amplitude does in agreement with the ESL determined by picosecond fluorescence (see above).

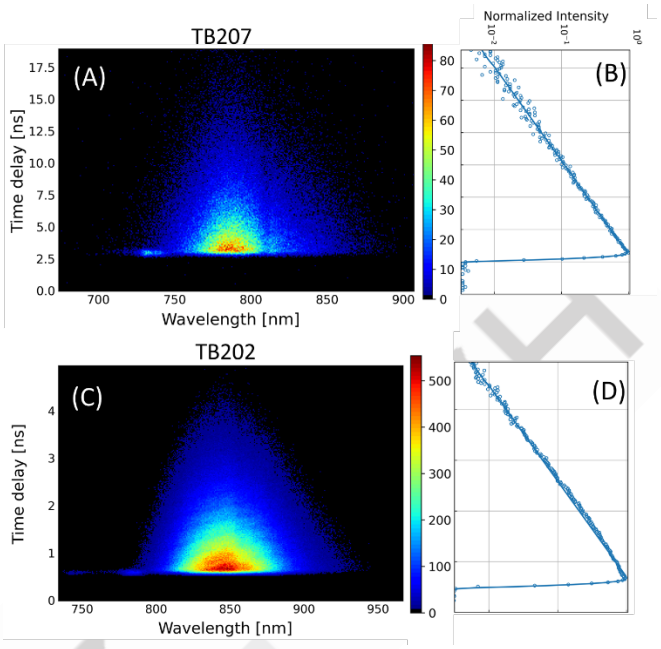

Figure 2. Time-gated streak camera images of **TB207**(A) and **TB202** dyes (B) in EtOH. Fluorescence detected in magic angle configuration. Note the difference in time scales for TB207 (20ns, 0.2 ns resolution) and TB202 (5 ns, 50 ps resolution). The normalized kinetic traces at the emission maximum are plotted for TB207 (B) and TB202 (D) with open circles for the data points and a straight line for the fitted mono-exponential function.

One can notice that the positive ΔA due to excited state absorption (ESA) is typically 10 times smaller in amplitude than the negative ΔA, due to ground state bleach (GSB, 710-800 for **TB207** and 760-820 nm for **TB202**) and stimulated emission (SE, > 760 nm for **TB207** and >800 nm for **TB202**). The ESA spectrum most likely extends over the whole wavelength range (440-1030 nm). The comparison of the SE amplitude with the steady-state fluorescence spectrum (SSE) shows that the former is reduced in the range of 800-900 nm (**TB207**) or 850-950nm (**TB202**), indicating a positive ESA at these wavelengths. It is likely, but not certain that a similar compensation acts also in the GSB region. We note that ESA shows up in these spectra as two positive bands extending from 440 to 700 and from 890 to 1030 nm, and we expect these same features and band shapes to be present in the DSSC TAS data.

The ESL lifetimes obtained for **TB207** from the fits (34 ± 3 ps and 2.7 ± 0.5 ns) of these data are in good agreement with the values obtained from time-resolved fluorescence (table 1). The shorter 34 ps component is due to excited state relaxation, also observed by fluorescence up-conversion with 150 fs time resolution (see SI, discussed above), and the second one has a large error bar due to the limited time range scanned (4 ns).

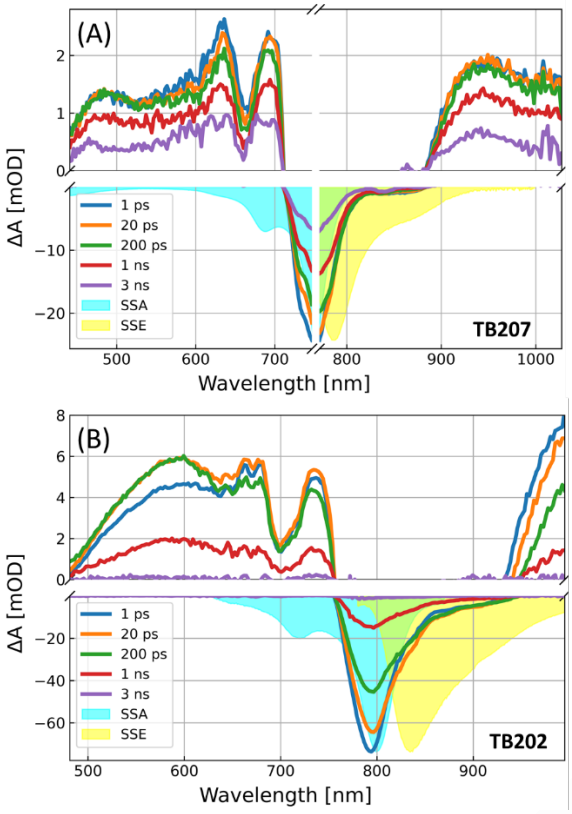

Figure 3. TAS of TB207 (A) and TB202 (B) dyes in EtOH. TAS spectra are compared to the inverted spectrum of the steady-state absorption (SSA) and steady-state emission (SSE). A positive sign signal indicates increased excitation-induced absorbance, while negative signals are due to either decreased absorbance or stimulated emission.

Table 1. Fluorescence decay times of **TB202** and **TB207** in EtOH measured by Streak camera and **TB207** cells measured with fluorescence up-conversion. For the data from TiO_2 and Al_2O_3 cells, the lifetimes were obtained by fitting a modified stretched exponential function (eq. 2) [39]. A typical error of 3% applies to all quantities.

Sample	τ_0	β	Av. decay rate <k> (ns^{-1})
TB207 Solution (Streak camera)	3.1 ns	-	0.323
TB202 Solution (Streak camera)	0.82 ns	-	1.22
TB207 Al_2O_3 0 mM CDCA (Up-conversion)	3.8 ps	0.3	79
TB207 TiO_2 5 mM CDCA (Up-conversion)	2.9 ps	0.4	138

Aggregation of dyes grafted on TiO_2 and Al_2O_3

Proto-type DSSCs devices with 10x10 mm^2 active areas were assembled with electrolyte composition and other material details described in the "experimental section". A 0.1 mM dye solution was used for the grafting of both the **TB202** and **TB207** samples. Because both dyes are perfectly symmetrical, they do not exert any noticeable interfacial dipole moment which could influence the electrostatic equilibrium with the TiO_2 density of states. This is also verified experimentally by charge extraction technique showing that neither the distribution of density of states nor the energetics of the TiO_2 conduction band edge is affected by the structural change of two dyes (Figure S14).

Aggregation of dyes leads to broadening of the absorption spectra as highlighted in figure 4 for **TB202** and **TB207** on TiO_2. The spectra of the Al_2O_3 cells are given in Figures S2. Co-adsorbing cheno-deoxycholic acid (CDCA) increases the average distance between monomers and thus reduces the aggregate concentration as indicated by a reduced absorption on the high and low energy sides for higher CDCA concentration and in comparison with the aggregate-free solution spectra. In the following, we will refer to the aggregates as dimers since they are statistically the most abundant form (monomer absorption is the major component in the spectra, even for 0mM CDCA, fig. 4).

We note that these dimer-related features are more pronounced for grafting on TiO_2 than for Al_2O_3 for **TB207** (see fig. S2), which is an important point to keep in mind when cells with equal aggregate concentrations are to be compared (*vide infra*). Figure 5 displays the aggregate-only absorption bands obtained from total spectra after subtraction of the one of solution, scaled with the arbitrary assumption that the difference should be zero at the peak of the monomer absorption.

It is important to underline that both dimer transitions are optically active, which suggests that the monomers are most likely in an oblique side-by-side arrangement with a certain tilt angle α between them [40,41]. This is the most reasonable scenario, since the anchoring groups of all dyes are located on the molecular edges, implying a grafting configuration in which the dyes are exposed to interaction with the parallel planes of the neighboring ones (excluding J-aggregate arrangement, θ=0°, see SI). We note that when these difference spectra are normalized to the maximum of the low energy aggregate peak (fig. 5), for higher CDCA concentrations the high energy aggregate band loses intensity. This indicates that α is changing as a function of CDCA concentration.

A quantitative analysis of the aggregate spectra based on Kasha's theory [18,42,43] shows for TB207 that α increases from 85° at zero CDCA concentration to ≈110° for 10 mM of CDCA (see SI). This is most likely due to an increasing distance between the COO- anchoring groups on the surface of the SC nano-particles since for higher concentrations more CDCA intercalates. The average monomer distance in a dimer, measured between the molecular centers, is CDCA concentration-independent: 18.5-19 Å, but this is in agreement with the observation that the energy splitting, the Davidov splitting, expressing the distance-dependent dipole-dipole is constant for all CDCA concentrations. Finally, we note that the low energy absorption band of the aggregates with a peak at 790 nm is perfectly in resonance with the emission spectrum of the monomers, thus optimizing the rates for monomer-to-aggregate energy transfer (ET).

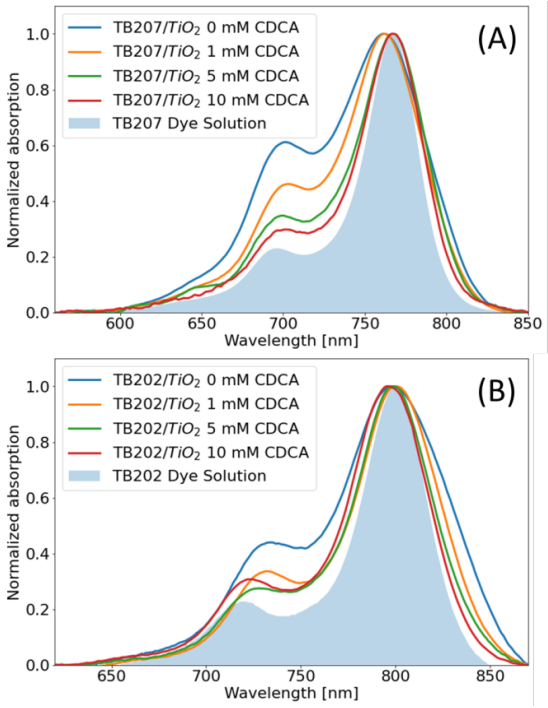

Figure 4. Normalized absorption spectra of TB207(A) and TB 202(B) TiO_2 solar cells. Blue areas are the steady-state absorption spectra of the solution.

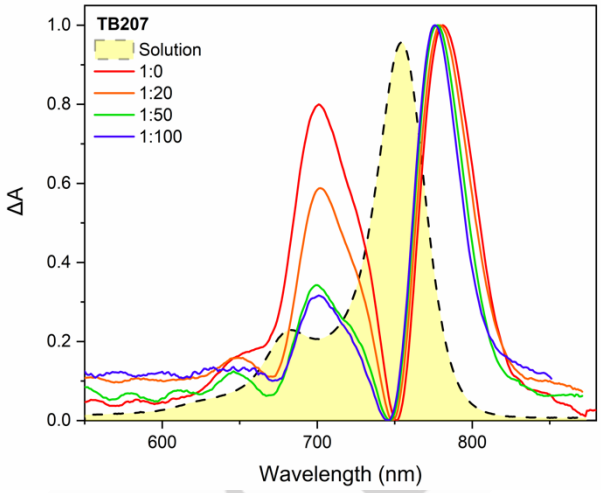

Figure 5. Aggregate absorption spectra ($\Delta A = A_{DSSC} - A_{solution}$) extracted from the total TB207/TiO_2 DSSCs, for increasing CDCA concentration by subtracting the corresponding absorption spectra in solution. Dashed line is the steady-state monomer absorption spectrum (solution).

Effect of aggregation on excited state dynamics of TB207 grafted on TiO_2 and Al_2O_3

The ET process is evidenced by a reduction of the fluorescence lifetime when **TB207** is grafted on Al_2O_3. Since the conduction band edge of Al_2O_3 is ≈ 0.41 eV higher in energy than for TiO_2, electron injection is impossible (the LUMO of **TB207** is only -ΔG= 0.1 eV above the CB edge of TiO_2) and the reduced ESL is due to ET only. The latter effect considerably reduces the ESL, as shown in Figure 6 for **TB207**/Al_2O_3 with 0 mM CDCA, where the fluorescence intensity is reduced by 50% within 5 ps. The time-resolved spectra (panel B) are almost delay-independent, apart from a slight 5-10 nm redshift in the first 5 ps, due to excited state relaxation. The kinetic traces in panel C show consistently a faster initial decay for the 780 and 800 nm traces. Due to the structural heterogeneity of the monomer-to-aggregate distances and relative orientations, ET rates are expected to span a large range of values. We approximate these decays with a modified version of the standard stretched exponential function[39] described by equation (2):

$$I(t) = \exp\left(1 - \left(1 + \frac{t}{\tau_0}\right)^{\beta}\right) * IRF(t) \qquad (2)$$

Eq. (2) corrects a major failure of the classical Kohlrausch function, for which the average decay rate $\langle k \rangle = k(t=0)$ diverges[39]. With eq. (2), it follows $\langle k \rangle = k(t=0) = \frac{\beta}{\tau_0}$ [39]. Furthermore, the fitting parameter τ_0 is related to the ensemble average ESL by $\langle \tau \rangle = \tau_0 \frac{e}{\beta} \Gamma\left(\frac{1}{\beta}, 1\right)$ [39] where Γ is the incomplete gamma function.

Table 1 gives the fitting parameters in detail, for the 800 nm trace, and also for the 5 mM CDCA/TiO_2 device. We note that due to monomer-to-dimer ET in the **TB207**/Al_2O_3 device, <k> is increased by more than a factor of 100, as compared to the **TB207** solution. For comparison, table ST1 gives the result of a 3-exp. fit (average lifetime $\langle \tau \rangle$ =54ps).

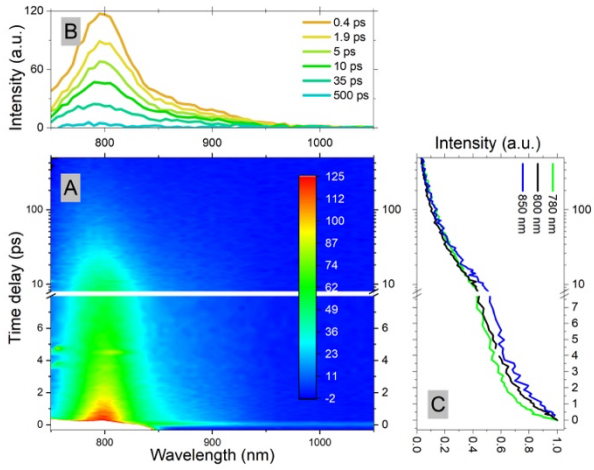

Figure 6. Broadband fluorescence up-conversion data for **TB207**/Al_2O_3 with 0 mM CDCA, and excited at 730 nm. A: Time-and wavelength resolved data; B: Emission spectra as a function of delay; C: Normalized fluorescence kinetics at selected wavelengths. Data are averaged within ±5 nm around the central wavelength indicated. Note the break in the time axis at 8 ps. The scale is logarithmic thereafter. The Al_2O_3 layer induces very intense laser pump pulse scattering which shows up as the white area (> 1000 cts) for delays up to 0.3 ps, masking the initial fluorescence. Internal reflections of the pump pulse show up as weaker replica at 3.7 and 4.6 ps.

Femtosecond TAS reveals then the spectral signature of ET, namely the absorption spectrum of the excited dimers (Agg*). To this end, Figure 7A shows the time-resolved ΔA spectra for **TB207**/0 mM-CDCA/Al_2O_3 (2 and 5 mM in Figure S3).

At short delay times (< 1 ps) the positive ΔA at < 700 and > 850 nm can be attributed dominantly to monomer ESA, due to its resemblance with the corresponding spectra obtained for the dyes in solution (fig. 3). Fluorescence data indicated that the excited state decays by ≈ 60% within 10 ps (fig. 6). The near-IR part of ESA(mono) and the GSB decay indeed within that time

interval, and a prominent absorption band rises, with a peak at 870-80 nm, which we assign to ESA from aggregates, ESA(Agg*). While the spectrum in the VIS hardly changes in amplitude it slightly blue-shifts in the first 10 ps, i.e. during the rise time of ESA(Agg*). The remaining ESA with a peak at 620 nm then decays like the ESA at 880nm, meaning that both features characterize ESA(Agg*). The decay of Agg* occurs on a few hundreds of ps. Kinetic traces at selected wavelengths are plotted in Figure S4 for **TB207**/Al_2O_3 at different CDCA concentrations, together with the FLUPS decay kinetics for 0 and 5mM CDCA. Since fitting with stretched exponentials is not adequate for TAS data with overlaying species- or state-specific bands, we simply perform multi-exponential fits for selected wavelengths. The decay times are summarized in Table S1, indicating a difference of the SE/GSB trace with the fluorescence decay times for 0 and 5mM CDCA. This is due to the former probing partly the slower ground state recovery since the Agg* lifetime is longer than the monomer fluorescence. Clearly, for higher CDCA concentrations the ET transfer process slows down and the amplitude of ESA(Agg*) decreases due to the lower concentration of aggregates (see fig. S3 for the spectra with 2 and 5 mM CDCA). When we assume that all the spectral features decay with the same set of four time constants (global fit), we obtain the decay-associated difference spectra (DADS), which are presented for 0mM CDCA in figure S5A together with a schematic allowing to identify the spectral signatures from monomer and aggregate excited states.

From these global fits, as well as from the fits of individual kinetic traces (table ST1), it is clear that ET transfer is slowed down for higher CDCA concentrations since the average monomer-to-dimer distance increases. The excited dimers then decay with the lifetimes τ_3 and τ_4 (Table ST1 and global fit fig. S5), which are in 100ps – 2ns range. Molecular dimers are known to form intra-dimer CT states [16,44–46], and the resemblance of the red part (550-650 nm) of the ESA(Agg*) with the spectrum of the TB207+ cation (see below) points to it. The most likely explanation is that τ_3 and τ_4 would simply be the CT recombination times.

For the TB207/TiO_2 devices, the central question is then on which time scale carrier injection occurs, and if it is in kinetic competition with the average rate of ET[12,13,15]. By inspection of the CDCA-dependent absorption spectra (fig. 4), we see that the aggregate concentrations differ for both TiO_2 and Al_2O_3 at a given CDCA concentration [6]. Indeed, TiO_2 seems to have a higher binding affinity for **TB207**, which leads to a higher propensity of aggregate formation. We will focus now on 5 mM CDCA on TiO_2, which was identified as optimal for achieving the highest PCE values [6]. On Al_2O_3 an equivalent aggregate-to-monomer ratio is found for 0 mM CDCA [6].

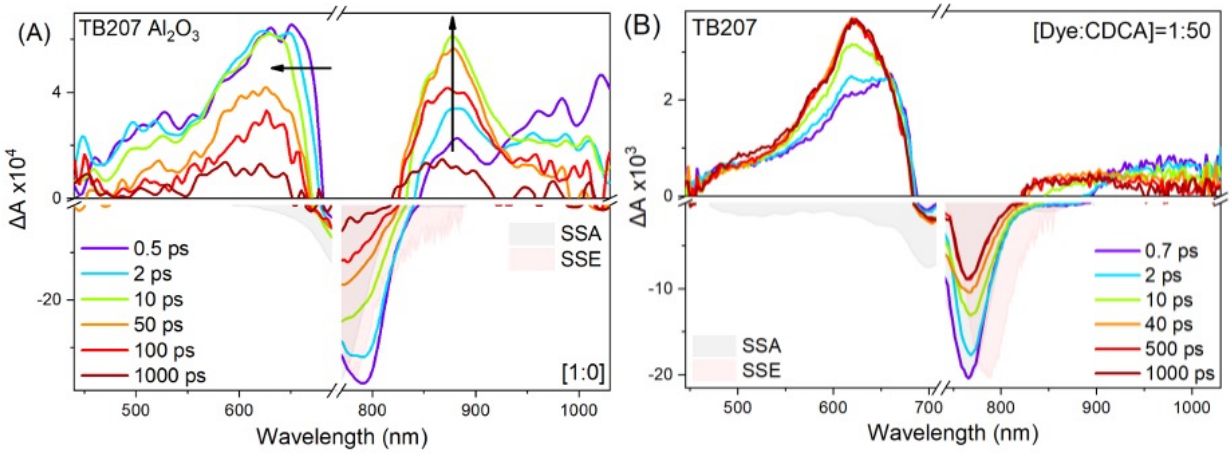

Figure 7. Time-resolved transient absorption spectra of **TB207** with 0 mM CDCA grafted on Al_2O_3 (A) and grafted on TiO_2 with 5mM CDCA. Excitation wavelengths 730 nm. Note the break on the x-axis at a wavelength interval of excessive pump light scattering, and the different scales on the y-axis for the negative and positive ΔA. The shaded SSA and SSE spectra are the sign-inverted steady-state absorption and fluorescence spectra. Excitation with average density of < 40 μJ/cm^2.

The fluorescence kinetics of both devices were analyzed using the modified Kohlrausch decay (cf. eq.(2)). The injection efficiency is given by the ratio of the ensemble-averaged rates for ET vs carrier injection (CT):

$$\eta_{inj} = 1 - \eta_{ET} = \frac{<k_{ET}>}{<k_{inj}>+<k_{ET}>}. \qquad (3)$$

Assuming the same $<k_{ET}>$ for the 5mM-CDCA/TiO_2 and the 0mM-CDCA/Al_2O_3 devices, $< k_{inj} > + < k_{ET} >$ is determined from the fluorescence decay of the former, and $<k_{ET}>$ from the latter (table 1). With this approach, we find η_{inj} = 0.64±0.05, in good agreement with the value obtained previously based on multi-exponential fits[6]. However, a different approach based on *temporally integrating* the time-dependent rates yields a lower injection efficiency of only 0.44 ± 0.05, as detailed in the Supp. Info. As outlined in Ref. [39], time-averaged (using the fluorescence decay as a distribution function) and ensemble-averaged rates are not the same. The relevant quantities for our discussion in the presence of structural heterogeneity are the ensemble-averaged rates, meaning that η_{inj} = 0.64±0.05, is the correct value.

In fig. 7B, the TAS spectra of **TB207**/5 mM-CDCA/TiO_2 show indeed a very prominent signature/absorption of the dye cation ($TB207^+$), with a peak at 625 nm. Note that its amplitude ΔA is completely formed at 40 ps and constant thereafter. In the near-IR (>850 nm), a weak and broad absorption is observed with the same kinetics, namely an increase of this absorption, or a transition from monomer-ESA to cation absorption within ≈ 10 ps, and a constant signal amplitude for delays ≥ 40 ps, indicating absence of charge recombination on the timescale probed

(3.5 ns). Analysing the ratio of GSB at time-zero and long-time delays at 770 nm ($\frac{\Delta A(t>3ns)}{\Delta A(t=0)}$), one can infer an injection yield of η_{inj} = 50 ± 10%, lower than the value obtained above (fluorescence decay)[6]. However, the determination by TAS is more inaccurate since the long-delay GSB amplitude is overlaid by cation absorption, and the time-zero GSB by stimulated emission, the amount of which can only be estimated.

Unlike the case of **TB207**/0mM-CDCA/Al_2O_3, the Agg* signatures do not show up, apart from a weak absorption at 850-900 nm in the 10 ps spectrum. This is line with the fact that CT wins over ET (see above), but the small amplitude of ESA(Agg*) is surprising.

For lower CDCA concentrations (0 and 2 mM), the TAS spectra and kinetic traces can be found Figure S6 in the SI. For 0mM CDCA, the ESA(Agg*) appears within the first ps, already present at a delay of 0.7 ps, attesting for the ET transfer process to dominate carrier injection. Nevertheless, the cation-type temporally constant absorption spectra are observed for t≥ 200 ps, when the ESA(Agg*) contribution has decayed. Figures S7 shows the CDCA-dependent kinetic traces for **TB207**/TiO_2, for characteristic wavelengths, such as 620 nm (cation max.), 780 nm (GSB/SE), 880 nm (max. of ESA(Agg*)/tail of cation absorption). For increasing CDCA concentration, the qualitative trends of ESA(Agg*) suppression and reduction of $<k_{ET}>$, i.e. an increasing rise time of ESA(Agg*) are apparent. We analyzed the kinetics by single wavelength and global fits, the results of which being summarized in (table SI). The decay-associated difference spectra (DADS) allow to identify the processes, which dominate for the different time scales, and as a function of CDCA. Since the excited state or photo-induced absorption spectra overlay in wavelength and time, this discussion is relatively involved and the reader is referred to the Supp. Info. for the details.

Nevertheless, the reaction scheme that emerges from the analysis of the DADS for **TB207**/5mM-CDCA/TiO_2 is summarized in the scheme below with the relevant time scales.

$$TB207 \xrightarrow{h\nu \leq IRF} TB207^{*LE} \xrightarrow{0.2-2\ \mathrm{ps}} TB207^{*} \begin{cases} \xrightarrow{2.8-23ps} TB207^{+} \\ \xrightarrow[5-40ps]{} \mathrm{Agg}^{*} \xrightarrow{0.1-2ns} TB207 \end{cases}$$

Scheme1: General reaction scheme for **TB207**/TiO_2 with lifetimes obtained for 5mM CDCA, i.e. the best device conditions. After excitation with 50 fs pulses, the local excited state TB207*^{LE} undergoes vibrational relaxation and forms TB207*. Electron injection forming the $TB207^+$ cation and energy transfer yielding Agg* compete since they occur on similar timescales (numbers taken from the global fits, see fig. S5). The latter decay back to the aggregate ground state (Agg), most probably due to recombination of the inter-aggregate CT state. $TB207^+$ cations are stable on the time scales probed (≤ 5 ns). Note that the same CT/ET branching reaction scheme holds for TB202.

Excited state dynamics of TB202 grafted on TiO_2 and Al_2O_3: Effect of aggregation and charge transfer driving force

The femtosecond TAS was performed with higher wavelength excitation at 770 nm, due to the red-shifted absorption spectra of **TB202** compared to **TB207**. The time-resolved ΔA spectra for **TB202**/10mM-CDCA/Al_2O_3 and **TB202**/10mM-CDCA/TiO_2 are displayed on Figure 8A and B (0,1 and 5 mM in SI). For **TB202,** the absorption spectra on Al_2O_3 and TiO_2 (fig. 4 and S2) indicate indeed similar aggregate/dimer concentrations for the same CDCA concentrations, unlike **TB207.** Ground state bleach (GSB, 795 nm) and stimulated emission (SE, 820 nm) signatures in the TAS measurement can be identified by comparison with the steady-state absorption and fluorescence spectra, respectively (plotted with inverted sign in fig. 8). Guided by the signatures of the monomer ESA signal of the **TB202** solution (fig. 3B), excited state absorption (ESA) can be identified for both DSSCs with maxima at 680 and 1000 nm. No CT can occur in Al_2O_3 cells, consequently we can attribute the longer lifetime component (>20 ps) to the absorption spectrum of the excited aggregate (Agg*).The spectra do not fully decay on the timescale of the measurement, which could indicate that ET leads to an intra-aggregate CT state [38], which decays on a nanosecond time scale, as for **TB207**. This is supported by the spectral resemblance of ΔA(Agg*) and the cation differential spectra observed for **TB202**/TiO_2(fig. 8B).

Table 2. TAS decay times of **TB202** in TiO_2 and Al_2O_3 cells with different CDCA concentrations, obtained by a global fit analysis. Although the fitting uncertainties are much smaller, an 20 fs error applies for τ_1 , which is close to the time resolution. We estimate a 3-5 % systematic error forτ_2 & τ_3, and 10 % for τ_4.

Semiconductor	TB202: CDCA	τ_1 (ps)	τ_2 (ps)	τ_3 (ps)	τ_4 (ps)	τ_5 (ps)
Al_2O_3	1:0	0.065	1.4	8.5	140	∞
	1:10	0.093	2	18	280	∞
	1:50	0.28	5.1	68	580	∞
	1:100	0.29	7	77	570	∞
TiO_2	1:0	0.88	5.3	48	500	∞
	1:10	0.21	3.9	40	250	∞
	1:50	0.21	4.4	46	410	∞
	1:100	0.26	2.8	49	180	∞

In the TiO_2 DSSC, and for delays ≤ 20 ps, GSB, SE and the monomer ESA occur at the same wavelengths as for Al_2O_3 (fig. 8B). For later delays, the prominent absorption spectrum of the cation (TB202+) appears at high (10 mM) CDCA concentration as an absorption band between 520-700 nm, with a maximum at 580 nm, and a weaker flat band ranging from 870 nm into the near IR. As the dye-regeneration operates on the ms timescale only[6], the cation spectra persist at longer timescale (>200 ps), while the absorption spectrum of the excited aggregate decays as witnessed for the Al_2O_3 cells. Note the slower rise time of the cation signature for **TB202**, as compared to **TB207** (fig. 7B).

Due to the spectral overlap of absorption of Agg* and TB202+, both contributions are impossible to separate. However, the partial decay and reshaping of □A in the VIS and near-IR portions

in the 200 ps to 1 ns time range may indicate decay of Agg* also for TiO_2, as observed in fig. 8A for the Al_2O_3 device.

To determine the lifetimes for CT and ET at different CDCA concentrations, we performed a global analysis of the TAS data, under the assumption that the kinetics are described by a set of wavelength-independent time constants using the variable projection (VARPRO) algorithm.[47] Best agreement is obtained when the TAS of the solar cells are fitted with a minimum of 4 components and an infinite lifetime component, as shown in table 2. The corresponding DADS are displayed in fig. S13.

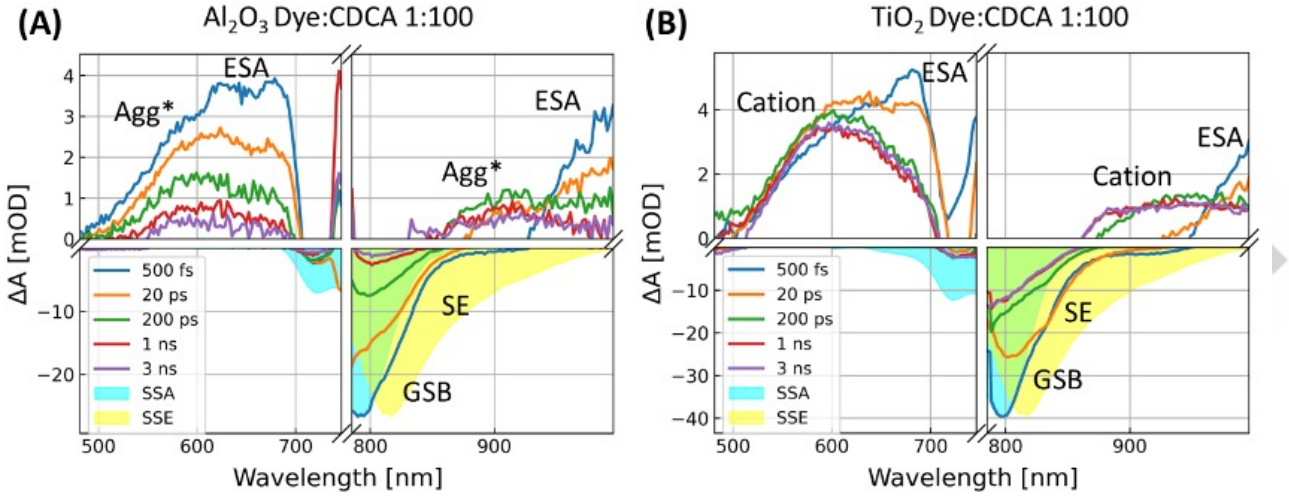

Figure 8. Time-resolved transient absorption spectra of **TB202** with 10 mM CDCA grafted on Al_2O_3 (A) and grafted on TiO_2 with 10 mM CDCA (B). Excitation wavelengths 770 nm. A break on the x-axis was introduced at a wavelength interval of excessive pump light scattering, and different scales are used for the y-axis for the negative and positive ΔA values. The shaded SSA and SSE spectra are the sign-inverted steady-state absorption and fluorescence spectra.

These lifetimes can be associated with processes by observing the corresponding DADS (cf. fig. S13). A reaction scheme similar to **TB207** (scheme 1) emerges, but with different lifetimes. For the Al_2O_3 cells ET transfer occurs on τ_2/τ_3 timescales. These values are increasing with the CDCA concentration, as the intermolecular distance between the monomers and the aggregates increases. The Agg* state decays with τ_4/τ_5 timescales back to the ground state, due to recombination of the inter-dimer CT state. For the TiO_2 cells CT and ET cannot be separated as they spectrally overlap and they both occur on τ_2/τ_3 timescales. On τ_4 timescale Agg* state decays, while the cation lifetime of τ_5 is longer than 3.5 ns (fitted as infinite).

Indeed, comparing these results to the lifetimes of **TB207** both ET and CT processes are slower, for comparable CDCA concentrations. The lifetimes associated with ET for Al_2O_3 samples (τ_2/τ_3 = 7 – 77 ps for 10 mM CDCA cell) are slower than the lifetimes of TiO_2 samples when both CT and ET take place in parallel (τ_2/τ_3 = 2.8 – 49 ps for 10 mM CDCA cell). The injection yield was determined for **TB202**/10mM-CDCA/TiO2 cell to be η_{inj} = 32 ± 10%, by calculating the ratio of GSB at time-zero and long time delays at 830 nm[7].The PCE of **TB202** is 2.5-times smaller than the PCE of **TB207**[7]. For the present 10 mM CDCA we find that ET is slower than for **TB207**, but the charge injection time is not fast enough to out-compete ET. Indeed, the main problem of the thienylated **TB202** is the lower driving force -ΔG = 0.02 eV[7] as compared to **TB207** (0.10 eV)[6].

Conclusions

The present femtosecond experiments allow to determine the relevant time scales and average rates, related to carrier injection and monomer-to-aggregate energy transfer, for both dyes. The analysis is complicated by the structural heterogeneity of the monomer and aggregate geometries, leading to an inhomogeneous distribution of lifetimes. This is best addressed for the fluorescence decay kinetics by the modified Kohlrausch function (eq.2), but for the TAS data a sum of exponentials has to be used. The SI show both global fits and single wavelength fits, which indicate the relevant time scales, but also the systematic errors in both approaches.

Nevertheless, the main picture that emerges is that the principal difference in PCE of devices made with both dyes comes indeed from the lower driving force -ΔG of **TB202,** which results in carrier injection and quenching by ET to occur on the same time scale, thus severely limiting the injection efficiency to ≈35%. **TB202** has indeed a more red-shifted absorption spectrum affording a larger AVT, but at the cost of a reduced LUMO energy and hence a too low -ΔG. In our devices, the effective -ΔG is increased by the addition of 1M Li+ ions in the electrolyte, but the shift is apparently not sufficient to compensate for the intrinsic lower reduction potential of **TB202**[7].

While in previous DSSCs the monomer-to-aggregate ET was considered to be a pure quenching, i.e. loss channel, the case of **TB207** questions this assumption. Indeed, the PCE is only weakly reduced to 3.0% at 0mM CDCA, as compared to 3.9% at 5mM CDCA (best device conditions), and J_{sc} is relatively, i.e. in the range of 16mJ/cm^2, even for 0 mM CDCA [6]. However, without any CDCA, the TAS data are dominated by the ESA(Agg*) signature and cations are emerging only at long delay times with a low ΔA amplitude (fig. S6), indicating a significantly lower cation concentration than at higher CDCA concentrations. This indicates that the low energy dimer state might possibly have enough driving force to contribute to carrier injection, yet on a slower time scale than the monomers. Some experiments were conducted on different near-IR dyes, as a function of the excitation wavelengths, in particular exciting the low energy edge of the absorption

spectra, where the aggregate concentration dominates[48]. The effect on the injection efficiency was nevertheless not convincingly detectable. Our next step will therefore be to conduct two-dimensional electronic spectroscopy with broadband excitation around 750 nm[49], which should allow us to detect the photo-induced cation concentration precisely as a function of the excitation wavelength[50].

Experimental section

Steady-state absorption spectra were recorded on a LAMBDA 950 UV/Vis spectrometer from PerkinElmer. The steady-state emission was measured using an Edinburgh instrument FLS920 Fluorescence spectrometer. The streak camera model that is used in our experiments is the HAMAMATSU C10627, mounted behind a spectrograph Jobin Yvon, 25-cm focal length, 50g/mm grating, blazed at 600 nm). The time resolution is 0.05 and 0.2 ns for streak camera delay ranges used for figure 2. Fluorescence detected in magic angle configuration.

Femtosecond set-ups. For both the time-resolved transient absorption and the fluorescence up-conversion setup (shown in S15) a Ti:sapphire laser system (FemtoLasers Synergy 20) was used. The laser pulses are amplified in a Chirped Pulsed Amplification with regenerative amplifier (Pulsar-Amplitude Technologies) resulting in a 0.5 mJ pulse energy, 800 nm central wavelength, 5 kHz repetition rate pulse train. The excitation wavelength is tuned to the absorption band of the DSSC's using a TOPAS-Prime (Light Conversion). The average pulse energy density (pulse energy/ ($1/e^2$ area)) of the excitation was chosen to prevent the signatures of exciton-exciton annihilation, which was observed in devices at higher energy densities[48]. For the **TB207** solution an energy density of ~ 60 μJ/cm^2 was used, but a lower energy density of ~ 30 μJ/cm^2 was required for the **TB207** DSSCs. In case of the **TB202** dye, the exciton-exciton annihilation effect appeared to be reduced. We could use average pulse energy densities of 260 μJ/cm^2 and ~ 80 μJ/cm^2 for the solution and the DSSCs, respectively. All data were recorded under magic angle conditions.

In the fluorescence up-conversion setup (see fig. S14) the pump excites the sample and the produced fluorescence is imaged onto a BBO crystal, by a pair of parabolic mirrors. Here the sum frequency is generated with a near-IR gate pulse (signal from TOPAS-Prime). The resulting up-converted signal is then detected as a function of gate-excitation delay by a LN_2-cooled CCD. The following conditions for SFG are optimized so as to obtain broadband phase-matching [51–53](> 100 nm for the present near-IR dyes): type II phase-matching with the gate beam in extra-ordinary polarization, ≈ 10° non-collinear angle between the gate beam and the center of the fluorescence cone, and a relatively thin 0.4 mm BBO crystal (cut at 25°).

Synthesis of TB207 and TB202. The protocol for the synthesis of both pyrrolopyrrole cyanine dyes is described in detail in Refs. 6 and 7, respectively. The 1H NMR and MALDI-TOF spectra are replicated in the Supp. Info of the present manuscript (Figs. S16-S19).

Sample preparation[48]**.** For the steady-state studies on dye solutions, these were prepared with lower optical densities in the range of 0.1-0.3/mm, in order to avoid reabsorption in fluorescence experiments. Higher OD values are used for the TAS and FLUPS measurements (0.3-0.55/mm). Spectroscopy grade ethanol was purchased from Sigma-Aldrich and used as received.

The DSSCs were prepared for both dyes following the protocol detailed here. The anodes are TEC11-type conductive glasses coated with a fluorine doped tin oxide (FTO) layer. The ≈4 μm thick semiconductor layer was deposited by screen printing. The TiO_2 coated anodes were heated up gradually to 500°C in an oven, while the Al_2O_3 covered anodes were heated up to 300°C and kept at these temperatures for half an hour. Then they were dipped overnight (15-17 h) in a dye solution (0.1 mM dye, 90% EtOH 10% $CHCl_3$). The cathodes are TEC11-type conductive glasses coated with FTO. Small diameter (<1 mm) holes allow the electrolyte to be injected by vacuum back-filling at the final stage of assembly. Cathodes were cleaned before assembly by three consecutive ultrasonic baths (1x15 min Acetone, 2x15 min EtOH). A transparent surlyn polymer holey square (12*12 mm outer size and 10-10 mm inner size) is placed between the anode and the cathode to glue the two electrodes together on a hot plate at 120°C melting the surlyn. The resulting cavity was filled with an acetonitrile-based PV-grade electrolyte provided by G-Lyte (Amiens, France). It contains 1 M LiI (lithium iodide), 1 M DMII (1,3-dimethylimidazole iodide) and 0.3 M I_2 (iodine). After electrolyte injection, the holes are sealed with thin cover slip glasses, and melted surlyn.

The DSSCs displayed optical densities at the peak absorbance in the range of OD=0.4 – 1.0, with the lower values corresponding to 50 or 100 mM CDCA. A background OD of ≈0.06-0.08 due to air-glass reflectivity and scattering by the semiconductor nanoparticles was subtracted.

Supporting Information

The supporting information contain additional tables and figures, the determination of the structural parameters of the aggregate dimers, as well as the calculation of the injection efficiency for **TB207** based on time-averaged fluorescence decay rates (as opposed to the appropriate ensemble averaging).

The authors have cited additional references within the Supporting Information[54–57].

Acknowledgements

We would like to express our thanks to F. Barath and his team (G-Lyte, Amiens) for providing components for the DSSCs. Furthermore, we thank L. Charbonnière (ICPEES) for giving access to the Edinburgh near-IR fluorimeter, and J. Léonard for insightful discussions. The Strasbourg team is grateful to Dr. O. Crégut for expert help in laser maintenance and development of data acquisition software, and for the funding provided by the ITI 2021-28 program of the University of Strasbourg, CNRS and Inserm, supported by IdEx Unistra (ANR 10 IDEX 0002), by SFRI STRAT'US project (ANR 20 SFRI 0012) and EUR QMAT ANR-17-EURE-0024 under the framework of the French Investments for the Future Program. This collaborative work has been carried out within the frame of the VISION-NIR project funded by "Agence Nationale de la Recherche" (ANR, grant agreement number ANR-17-CE05-0017). FS and FG also acknowledge the IMPRESSIVE

project, which received funding from the EU grant agreement no. 826013.

Keywords: near-IR DSSC, pyrrolopyrrole cyanines, charge transfer, energy transfer, molecular dimers, ultrafast, transient absorption, broadband fluorescence up-conversion

References

[1] R. R. Lunt and V. Bulovic, *Appl. Phys. Lett.* **2011,** *98*, 113305.
[2] C. J. Traverse, R. Pandey, M. C. Barr and R. R. Lunt, *Nat. Energy* **2017,** *2*, 849–860.
[3] A. D. Wulansari, D. Hayati, D. X. Long, K. Choi and J. Hong, *Sci. Rep.* **2023,** *13*, 1–11.
[4] C.-C. Chen, L. Dou, R. Zhu, C.-H. Chung, T.-B. Song, Y. B. Zheng, S. Hawks, G. Li, P. S. Weiss and Y. Yang, *ACS Nano* **2012,** *6*, 7185–7190.
[5] W. Naim, V. Novelli, I. Nikolinakos, N. Barbero, I. Dzeba, F. Grifoni, Y. Ren, T. Alnasser, A. Velardo and R. Borrelli, *Jacs Au* **2021,** *1*, 409–426.
[6] T. Baron, W. Naim, I. Nikolinakos, B. Andrin, Y. Pellegrin, D. Jacquemin, S. Haacke, F. Sauvage and F. Odobel, *Angew. Chem.* **2022,** *134*, e202207459.
[7] T. Baron, W. Naim, M. Kurucz, I. Nikolinakos, B. Andrin, Y. Pellegrin, D. Jacquemin, S. Haacke, F. Sauvage and F. Odobel, *J. Mater. Chem. A* **2023,** *11*, 16767–16775.
[8] R. R. Lunt, *Appl. Phys. Lett.* **2012,** *101*, 043902.
[9] F. Grifoni, M. Bonomo, W. Naim, N. Barbero, T. Alnasser, I. Dzeba, M. Giordano, A. Tsaturyan, M. Urbani, T. Torres, C. Barolo and F. Sauvage, *Adv. Energy Mater.* **2021,** *11*, 2101598.
[10] K. Zhang, C. Qin, X. Yang, A. Islam, S. Zhang, H. Chen and L. Han, *Adv. Energy Mater.* **2014,** *4*, 1301966.
[11] W. Naim, F. Grifoni, V. Challuri, D. Mathiron, S. Ceurstemont, P. Chotard, T. Alnasser, I. Dzeba, N. Barbero, S. Pilard, C. Barolo and F. Sauvage, *Cell Rep. Phys. Sci.* **2023,** *4*, 101455.
[12] K. Pydzińska and M. Ziółek, *Dyes Pigments* **2015,** *122*, 272–279.
[13] M. Ziólek, J. Karolczak, M. Zalas, Y. Hao, H. Tian and A. Douhal, *J. Phys. Chem. C* **2014,** *118*, 194–205.
[14] V. Novelli, N. Barbero, C. Barolo, G. Viscardi, M. Sliwa and F. Sauvage, *Phys Chem Chem Phys* **2017,** *19*, 27670–27681.
[15] C. Martín, M. Ziółek and A. Douhal, *J. Photochem. Photobiol. C Photochem. Rev.* **2016,** *26*, 1–30.
[16] H.-W. Bahng, A. Hagfeldt and J.-E. Moser, *J Phys Chem C* **2018,** 23.
[17] R. A. Marcus, *J. Chem. Phys.* **1956,** *24*, 966–978.
[18] Lanzani, Guglielmo, *The Photophysics behind Photovoltaics and Photonics*, Wiley-VCH Verlag GmbH, 2012, .
[19] H. Rensmo, K. Westermark, S. Södergren, O. Kohle, P. Persson, S. Lunell and H. Siegbahn, *J. Chem. Phys.* **1999,** *111*, 2744–2750.
[20] D. F. Watson and G. J. Meyer, *Coord. Chem. Rev.* **2004,** *248*, 1391–1406.
[21] Y. Bai, J. Zhang, Y. Wang, M. Zhang and P. Wang, *Langmuir* **2011,** *27*, 4749–4755.
[22] J. R. Jennings and Q. Wang, *J. Phys. Chem. C* **2010,** *114*, 1715–1724.
[23] S. Rühle, M. Greenshtein, S.-G. Chen, A. Merson, H. Pizem, C. S. Sukenik, D. Cahen and A. Zaban, *J. Phys. Chem. B* **2005,** *109*, 18907–18913.
[24] S. S. Pandey, S. Sakaguchi, Y. Yamaguchi and S. Hayase, *Org. Electron.* **2010,** *11*, 419–426.
[25] V. Sundström and A. Yartsev, in *Energy and Environment Series*, ed. P. Piotrowiak, Royal Society of Chemistry, Cambridge, 2013, , pp. 135–160.
[26] C. S. Ponseca, P. Chábera, J. Uhlig, P. Persson and V. Sundström, *Chem. Rev.* **2017,** *117*, 10940–11024.
[27] S. Ardo and G. J. Meyer, *Chem Soc Rev* **2009,** *38*, 115–164.
[28] T. Hannappel, B. Burfeindt, W. Storck and F. Willig, *J. Phys. Chem. B* **1997,** *101*, 6799–6802.
[29] H. N. Ghosh, J. B. Asbury and T. Lian, *J. Phys. Chem. B* **1998,** *102*, 6482–6486.
[30] G. Benkö, J. Kallioinen, J. E. I. Korppi-Tommola, A. P. Yartsev and V. Sundström, *J. Am. Chem. Soc.* **2002,** *124*, 489–493.
[31] R. Huber, J.-E. Moser, M. Grätzel and J. Wachtveitl, *J. Phys. Chem. B* **2002,** *106*, 6494–6499.
[32] K. Sunahara, A. Furube, R. Katoh, S. Mori, M. J. Griffith, G. G. Wallace, P. Wagner, D. L. Officer and A. J. Mozer, *J. Phys. Chem. C* **2011,** *115*, 22084–22088.
[33] N. A. Anderson and T. Lian, *Annu. Rev. Phys. Chem.* **2005,** *56*, 491–519.
[34] H. Němec, J. Rochford, O. Taratula, E. Galoppini, P. Kužel, T. Polívka, A. Yartsev and V. Sundström, *Phys. Rev. Lett.* **2010,** *104*, 197401.
[35] T. Geiger, I. Schoger, D. Rentsch, A. C. Véron, F. Oswald, T. Meyer and F. Nüesch, *Int. J. Photoenergy* **2014,** *2014*, e258984.
[36] J. Sobuś, J. Karolczak, D. Komar, J. A. Anta and M. Ziółek, *Dyes Pigments* **2015,** *113*, 692–701.
[37] A. Kaczmarek-Kedziera and D. Kędziera, *Theor. Chem. Acc.* **2016,** *135*, 1–17.
[38] H.-W. Bahng, A. Hagfeldt and J.-E. Moser, *J. Phys. Chem. C* **2018,** *122*, 19348–19358.
[39] M. Berberan-Santos, E. Bodunov and B. Valeur, *Chem. Phys.* **2005,** *315*, 171–182.
[40] A. R. Monahan and D. F. Blossey, *J. Phys. Chem.* **1970,** *74*, 4014–4021.

[41] P. Bojarski, A. Matczuk, C. Bojarski, A. Kawski, B. Kukliński, G. Zurkowska and H. Diehl, *Chem. Phys.* **1996,** *210*, 485–499.
[42] M. Kasha, *Radiat. Res.* **1963,** *20*, 55–70.
[43] N. J. Hestand and F. C. Spano, *Acc. Chem. Res.* **2017,** *50*, 341–350.
[44] Y. Hong, F. Schlosser, W. Kim, F. Würthner and D. Kim, *J. Am. Chem. Soc.* **2022,** *144*, 15539–15548.
[45] J. Sung, A. Nowak-Król, F. Schlosser, B. Fimmel, W. Kim, D. Kim and F. Würthner, *J. Am. Chem. Soc.* **2016,** *138*, 9029–9032.
[46] H.-W. Bahng, A. Hagfeldt and J.-E. Moser, *J Phys Chem C* **2018,** 19.
[47] D. P. O'Leary and B. W. Rust, *Comput. Optim. Appl.* **2013,** *54*, 579–593.
[48] Nikolinakos, Ilias, *Ultrafast Spectroscopy of Transparent Dye Sensitized Solar Cells Designed for the Near-Infrared*, PhD thesis, University of Strasbourg (**2022**), https://www.theses.fr/2022STRAE005.
[49] M. Gueye, J. Nillon, O. Crégut and J. Léonard, *Rev. Sci. Instrum.* **2016,** *87*, 093109.
[50] F. D. Fuller and J. P. Ogilvie, *Annu. Rev. Phys. Chem.* **2015,** *66*, 667–690.
[51] M. Gerecke, G. Bierhance, M. Gutmann, N. P. Ernsting and A. Rosspeintner, *Rev. Sci. Instrum.* **2016,** *87*, 053115.
[52] M. Sajadi, M. Quick and N. P. Ernsting, *Appl. Phys. Lett.* **2013,** *103*, 173514.
[53] L. Zhao, J. Luis Pérez Lustres, V. Farztdinov and N. P. Ernsting, *Phys Chem Chem Phys* **2005,** *7*, 1716–1725.
[54] M. Yu. Losytskyy, V. M. Yashchuk, S. S. Lukashov and S. M. Yarmoluk, *J. Fluoresc.* **2002,** *12*, 109–112.
[55] N. R. Reddy, S. Rhodes, Y. Ma and J. Fang, *Langmuir* **2020,** *36*, 13649–13655.
[56] C. M. Carbonaro, *J. Photochem. Photobiol. Chem.* **2011,** *222*, 56–63.
[57] F. del Monte, J. D. Mackenzie and D. Levy, *Langmuir* **2000,** *16*, 7377–7382.

Entry for the Table of Contents

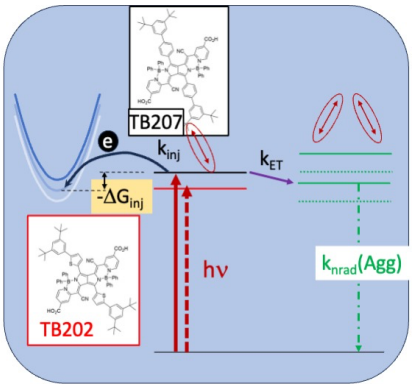

Near-IR dyes for transparent dye-sensitized solar cells: The effects of small driving forces (-ΔG) and excited state quenching by energy transfer to aggregates studied by femtosecond differential absorption and fluorescence spectroscopy for two DPP cyanine dyes.

Institute and/or researcher Twitter usernames: ((optional))